Continuous H_2O_2 production sustained by anodic O_2 for the destruction of the antibiotic ampicillin by photoelectro-Fenton process in a rotating cylinder electrode reactor

Oscar M. Cornejo[a], Ignasi Sirés[b,*], José L. Nava[a,**]

[a] *Departamento de Ingeniería Geomática e Hidráulica, Universidad de Guanajuato, Av. Juárez 77, Zona Centro, 36000, Guanajuato, Guanajuato, Mexico*

[b] *Laboratori d'Electroquímica dels Materials i del Medi Ambient, Departament de Ciència de Materials i Química Física, Secció de Química Física, Facultat de Química, Universitat de Barcelona, Martí i Franquès 1-11, 08028 Barcelona, Spain*

Paper submitted to be published in the

Journal of Environmental Chemical Engineering

* Corresponding author i.sires@ub.edu (I. Sirés)

** Corresponding author: jlnm@ugto.mx (J.L. Nava)

Abstract

In this work, the experimental characterization of a rotating cylinder electrode (RCE) reactor employed for the complete degradation of the antibiotic ampicillin (AMP) by photoelectro-Fenton (PEF) process has been addressed for the first time. Once produced from water oxidation at six Ti|IrO_2 anodic plates, O_2 was quickly transported by forced convection toward the central RCE, which consisted of a 316 stainless-steel cylinder covered with a (C-PTFE)-coated carbon cloth, thus ensuring the continuous production of H_2O_2 from the two-electron O_2 reduction reaction (ORR). The accumulated H_2O_2 reached a concentration of 83.3 mg L^{-1} H_2O_2 after 60 min in a 50 mM Na_2SO_4 solution at pH 3, operating at an RCE peripheral velocity U = 79.6 cm s^{-1} and fixed cathodic potential E_{cath} = −0.45 V vs. SHE. Furthermore, the optimum PEF conditions led to the complete destruction of 10 mg L^{-1} AMP in only 10 min upon addition of 0.4 mM Fe^{2+} as catalyst under UVA light irradiation, with a low electrolytic energy consumption of 0.211 kWh (g TOC)$^{-1}$. In addition, the evolution of final carboxylic acids and inorganic ions over the electrolysis time was monitored by chromatographic and spectrophotometric techniques. PEF treatment clearly outperformed the anodic oxidation with H_2O_2 and the electro-Fenton (EF) processes, which opens the door to a sustainable and powerful electrochemical technology with no need for an air compressor for H_2O_2 production and viable under limitless sunlight irradiation.

Keywords: Antibiotic residues; Electrochemical advanced oxidation processes; Hydrogen peroxide electrosynthesis; Oxygen reduction reaction; RCE reactor; Water treatment

1. Introduction

Antibiotics are one of humankind's greatest inventions, decisively contributing to increase both the lifespan and the quality of life by confronting lethal bacterial diseases [1]. However, the ever-growing demand and consumption of these pharmaceuticals have caused their uncontrolled discharge into water bodies, causing negative environmental impact [2,3]. Many countries have reported the presence of antibiotics in wastewater treatment plants (WWTPs) and surface water, at concentrations ranging from ng L^{-1} to μg L^{-1} [4-7].

Despite the low concentrations of these pollutants in the environment, some studies have shown their potential toxicity to aquatic organisms [3,8,9]. Furthermore, the worrisome expansion of antibiotic-resistant bacteria and genes poses a global health menace that must be considered a top-priority problem to be solved, as it endangers future wellness around the globe [3,8,9]. The prolonged presence of antibiotic residues with water empowers the pathogens [2,10-12], being urgent to develop more efficient strategies for the fast removal of these chemicals from wastewater [2,3,10,11,13,14].

In the last decade, the electrochemical advanced oxidation processes (EAOPs) have emerged as one of the most powerful approaches to eliminate pharmaceuticals from water [1,15-17]. EAOPs offer crucial advantages as compared to more conventional oxidation processes, as for example the in-situ generation of chemicals needed to carry out the reactions by easily modulating the electrolysis conditions [18,19]. The great performance of EAOPs arises from the generation of highly oxidizing agents, e.g., the hydroxyl radical ($^{\bullet}$OH), either directly on the anode surface (M) from water oxidation (reaction (1)) or indirectly through the electrosynthesis of chemicals that can be further activated to yield homogeneous $^{\bullet}$OH in the bulk solution [15,20]. In indirect EAOPs, the oxygen reduction reaction (ORR) occurs

through a two-electron pathway (reaction (2)) that yields H_2O_2 with high faradaic efficiency when carbonaceous cathodes are employed [20,21].

$$H_2O + M \rightarrow M(^{\bullet}OH) + H^+ + e^- \quad (1)$$

$$O_2 + 2H^+ + 2e^- \rightarrow H_2O_2 \quad (2)$$

The electro-Fenton (EF) process is the paradigm of indirect EAOPs, since H_2O_2 continuously electrogenerated from reaction (2) is immediately decomposed by a metal catalyst to yield $^{\bullet}OH$ via reaction (3), thereby being feasible to attain a fast scission of the backbone of organic molecules [21-23]. Additionally, the reduced form of the catalyst can be cathodically regenerated (reaction (4)), which is fundamental to sustain the $^{\bullet}OH$ production [1]. Moreover, the irradiation with UVA light in the so-called photoelectro-Fenton (PEF) process promotes the photoreduction of photosensitive refractory Fe(III)-organic complexes (reaction (5)) and Fe(III)-hydroxocomplexes (reaction (6)) formed along the treatment, thereby feeding the Fenton's reaction (3) continuously [24-27].

$$H_2O_2 + Fe^{2+} \rightarrow Fe^{3+} + {}^{\bullet}OH + OH^- \quad (3)$$

$$Fe^{3+} + e^- \rightarrow Fe^{2+} \quad (4)$$

$$[Fe(OOCR)]^{2+} + h\nu \rightarrow Fe^{2+} + CO_2 + R^{\bullet} \quad (5)$$

$$[Fe(OH)]^{2+} + h\nu \rightarrow Fe^{2+} + {}^{\bullet}OH \quad (6)$$

The H_2O_2 electrosynthesis is the most distinct feature of EF and PEF processes, as a sufficiently high H_2O_2 concentration ensures a good degradation performance. It is well established that the ORR is very efficient with carbonaceous materials assembled in gas-diffusion electrodes (GDEs) [28-32]. Nevertheless, the GDE configuration compels the use of an air compressor to fulfill the O_2 demand needed to carry out the ORR, which increases the energy consumption of the process.

On the other hand, the contribution of the anode material in EF and PEF to the elimination of pollutants is usually modest, since homogeneous $^{\bullet}$OH generated through Fenton's reaction (3) is much more abundant, available and reactive than the M($^{\bullet}$OH) confined at the anode surface (reaction (1)) [33,34]. Most cell configurations for these applications are assembled using active anodes that favor the oxygen evolution reaction (OER, reaction (7)), being typically considered a detrimental reaction. Nonetheless, a well-designed electrochemical reactor can convert the electrolytic O_2 into a valuable resource to produce H_2O_2 from reaction (2), avoiding the use of an air compressor [35-37].

$$2H_2O \rightarrow O_2 + 4H^+ + 4e^- \quad (7)$$

One of our latest articles served as proof of concept of the advantageous interplay between OER and mass transport enhancement. The forced convection of dissolved anodic O_2 was characterized in terms of H_2O_2 accumulation from ORR at a rotating cylinder electrode (RCE) reactor operated in batch mode [38]. A plateau attributed to the mass-transport controlled H_2O_2 generation was identified at a cathodic potential of $-0.65 \leq E_{cath} \leq -0.3$ V vs. SHE. From this, potentiostatic trials were conducted to attain up to 5.2 mM H_2O_2, but no application to water treatment was developed.

To further expand the technologically relevant idea of self-sustained H_2O_2 electrosynthesis within the context of EAOPs, the use of a reactor equipped with a central carbon cloth-coated stainless-steel rotating cylinder to produce H_2O_2 via anodically-generated O_2 and further eliminate the antibiotic ampicillin (AMP) by PEF process in batch mode is shown for the first time. The influence of key parameters, including the added Fe^{2+} and drug concentrations and the RCE peripheral velocity (U), on the antibiotic degradation was systematically analyzed. Bulk electrolytic trials were performed at E_{cath} = -0.45 V vs.

SHE to ensure that the ORR was controlled by mass transport. The evolution of final products, such as carboxylic acids and inorganic ions, was monitored during the trials.

2. Material and methods

2.1 Chemicals

Ampicillin ($C_{16}H_{19}N_3O_4S$; CAS No.: 69-53-4; molecular weight: 349.40 g mol^{-1}; purity > 96%) was supplied by Sigma-Aldrich (see structure in Fig. 1). Analytical grade Na_2SO_4 (purity > 99%) employed as supporting electrolyte was obtained from Karal, whereas concentrated H_2SO_4 solution (Reag. Ph. Eur., 96%) required for initial pH adjustment was purchased from PanReac AppliChem ITW Reagents. Other chemicals for analytical determinations were supplied by Sigma-Aldrich. Solutions to carry out the analyses and electrolytic trials were prepared with double-distilled water. Reagents needed for the mobile phase and organic solvents were of high-performance liquid chromatography (HPLC) grade.

2.2 Experimental set-up

The isometric view of the RCE reactor is depicted in Fig. 2a. This system consisted of a glass beaker (inner diameter of 8.3 cm and height of 11.0 cm) filled with 500 mL of solution in each assay to be operated in batch mode. A rotating AISI 316 stainless-steel cylinder with dimensions of 3.8 cm (diameter) × 11.0 cm (length), resulting in an exposed surface area of 120 cm^2, was placed in the center of the beaker, once tightly covered with commercial C-PTFE-coated carbon cloth (Sainergy). On the other hand, six Ti $|$ IrO_2 plates with dimensions of 13.0 cm (length) × 2.0 cm (width) × 0.3 cm (thickness), resulting in a geometric area of 120 cm^2 in contact with the solution, were placed as the anodes concentrically with one of their sides supported on the internal wall of the beaker. The anodes, which were manufactured by the Pechini method as described previously [39], were fastened with screws,

giving rise to the arrangement depicted in the zenithal view of Fig. 2b. An electric motor from IKA (model RW 20) with 0.11 hp of power served to rotate the central coated cylinder. In each given trial, the cathode potential (E_{cath}) was kept constant by connecting the working RCE to a saturated mercury/mercurous sulfate reference electrode that was placed in the gap between the central cathode and one of the anodes. In this manuscript, all the electrode potentials have been converted to be referred to the standard hydrogen potential (SHE). In Fig. 2a, also note that the experimental set-up included a 6-W fluorescent black light blue tube from Philips, employed as UVA lamp (λ_{max} = 360 nm) in the PEF process. The experiments were always carried out in a black box, aiming to avoid the impact of environmental radiation when the electrolytic trials were performed with the UVA lamp turned off.

2.3 Bulk electrolytic trials in the RCE

In all the experiments, a constant E_{cath} = – 0.45 V vs. SHE was ensured by means of an SP 150 potentiostat-galvanostat, which was coupled to an external booster VMP3B-10 from BioLogic. The EC-Lab® software was employed to monitor the potential during the assays. It must be mentioned that this specific potential value was chosen to keep the ORR (reaction (2)) under mass transport control, on the basis of our recent investigation that demonstrated the existence of a plateau attributed to this reaction within the range $-0.65 \leq E_{cath} \leq -0.35$ V vs. SHE [38].

The accumulation of H_2O_2 was carried out in the electrochemical system described in subsection 2.1. For this study, solutions of 500 mL of 50 mM Na_2SO_4 were electrolyzed at pH 3 and 298 ± 2 K for 60 min. The influence of the peripheral velocity of the rotating cylinder ($U = 2\pi fr/60$, where f is in rpm, r denotes the RCE radius in cm, and 60 is a factor

149 to express U values in cm s^{-1}) on the accumulated H_2O_2 concentration over the electrolysis
150 time was evaluated within the U range from 11.9 to 79.6 cm s^{-1} (i.e., $60 \leq f \leq 400$ rpm). The
151 H_2O_2 concentration was quantified at each selected time by means of the Ti(IV)-H_2O_2
152 complex colorimetric method, employing a Perkin-Elmer Lambda 35 UV/Vis
153 spectrophotometer set at $\lambda = 408$ nm.

154 Bulk electrolytic trials with duration of 60 min were also performed to investigate the
155 AMP elimination by several EAOPs, using the same supporting electrolyte mentioned above
156 at pH 3. The influence of initial Fe^{2+} concentration (from 0.3 to 0.6 mM), U (from 11.9 to
157 79.6 cm s^{-1}) and initial AMP concentration (from 5 to 15 mg L^{-1}) was systematically assessed.
158 These assays were also carried out at a fixed E_{cath} = – 0.45 V vs. SHE. All data reported in
159 the graphs have been averaged from two analogous trials, thereby providing the error bars.

160 In the mineralization trials by the PEF process, the energy consumption per unit TOC
161 mass (EC_{TOC}, in kWh (g TOC)$^{-1}$) and mineralization current efficiency (MCE, in %) were
162 calculated as follows:

163 $$EC_{TOC} = \frac{E_{cell} I t}{V \Delta(TOC_{exp})} \quad (8)$$

164 $$MCE = \frac{n F V \Delta(TOC_{exp})}{4.32 \times 10^7 m I t} \times 100 \quad (9)$$

165 where E_{cell} is the cell voltage (V), I is the output current (A), t is the electrolysis time (h),
166 $\Delta(TOC)_{exp}$ is the TOC variation during the assay (mg L^{-1} TOC), n is the number of electrons
167 transferred during the mineralization of AMP solutions (reaction (10)), F is the Faraday
168 constant, m is the number of carbon atoms contained in each AMP molecule, and 4.32×10^7
169 is a conversion factor for dimensional homogeneity.

170 $$C_{17}H_{18}FN_3O_3 + 37H_2O \rightarrow 17CO_2 + F^- + 2NO_3^- + NH_4^+ + 88H^+ + 86e^- \quad (10)$$

171 *2.4 Analytical methods*

172 The Fe^{2+} concentration was quantified by the standard 1,10-phenanthroline colorimetric
173 procedure, measuring the absorbance at λ = 510 nm in the same spectrophotometer mentioned
174 above [40]. The AMP concentration was measured by HPLC in an Agilent Series 1200
175 chromatograph, which was equipped with a PDA detector and an Agilent SB-C18 1.8 µm,
176 50 mm × 2.1 mm (i.d.) column. An excellent AMP peak was identified at λ = 260 nm and
177 retention time of 1.8 min, after injecting 100 µL of the sample that were eluted with a mixture
178 of 90% water and 10% acetonitrile as mobile phase at 0.6 mL min^{-1}. The solution TOC
179 content was determined using a Teledyne Tekmar TOC Torch analyzer.

180 On the other hand, the carboxylic acids generated through the electrolysis were identified
181 and quantified by ion-exclusion HPLC with the same chromatographic device described
182 above, although equipped with an Agilent Hi-Plex H 8 mm, 300 mm × 7.7 mm (i.d.) column
183 and the PDA detector set at λ = 210 nm. For this analysis, 20 µL of the sample were injected
184 to be eluted by a 5 mM H_2SO_4 solution employed as mobile phase at 0.6 mL min^{-1}. From the
185 obtained chromatograms, two peaks were assigned to oxalic and oxamic acid at 9.0 and 13.2
186 min, respectively. Nitrate ion was monitored by injecting 20 µL of the sample into a Perkin
187 Elmer Flexar chromatograph equipped with a Shim-Pack IC-A1S, 100 mm × 4.6 mm, anionic
188 column at room temperature. The mobile phase was composed of a mixture of 2.4 mM
189 tris(hydroxymethyl)aminomethane (pH 4) and 2.6 mM phthalic acid, being eluted at 1.5 mL
190 min^{-1}. The resulting chromatograms exhibited two peaks at 1.9 and 13.5 min, attributed to
191 nitrate and sulfate ions, respectively, upon comparison with standards. On the other hand,
192 ammonium ion was analyzed using the standard indophenol blue colorimetric analysis, using
193 the aforementioned spectrophotometer set at λ = 630 nm [41].

3. Results and discussion

3.1 Self-sustained H_2O_2 production

The electrosynthesis of H_2O_2 from two-electron ORR (reaction (2)) is a primordial step in Fenton-based EAOPs, which are often superior to their non-electrochemical counterparts because the H_2O_2 is progressively supplied to the bulk solution, mimicking a stepwise addition that allows minimizing the parasitic scavenging of $^{\bullet}OH$ that typically occurs when an excess of H_2O_2 is supplied at once. Fig. 3a shows the influence of U in the range 11.9-79.6 cm s^{-1} on the H_2O_2 concentration accumulated from the reduction of the transported anodic O_2. As can be observed, at each sampling time, the concentration increases when operating at greater peripheral velocity, attaining 0.92 mM (31.3 mg L^{-1}), 1.21 mM (41.2 mg L^{-1}), 1.30 (44.3 mg L^{-1}), 1.99 mM (68 mg L^{-1}), and 2.45 mM (83.3 mg L^{-1}) of H_2O_2 at 11.9, 19.9, 39.8, 59.7, and 79.6 cm s^{-1}, respectively, after 60 min of electrolysis. It can be noticed that at $t \geq 20$ min, a semi-plateau is reached at $U \geq 11.9$ cm s^{-1}. This progressive deceleration of the H_2O_2 accumulation can be mainly attributed to two parasitic reactions, whose contribution becomes more relevant at higher H_2O_2 content: (i) the H_2O_2 reduction reaction (11); and (ii) the direct H_2O_2 oxidation at the anode surface (reverse of reaction (2)).

$$H_2O_2 + 2H^+ + 2e^- \rightarrow 2H_2O \quad (11)$$

The rising H_2O_2 concentration as U is increased can be explained by the faster mass transport (larger forced convection) of electrolytic O_2 towards the cathode surface promoted by its rotation. The accumulated H_2O_2 concentrations reached in this work at t = 60 min are in good agreement with those obtained in our previous article, in which the electrolytic trials were performed for 180 min [38]. Also, at higher U, the O_2 supersaturation in the solution is favored, which increases the amount of H_2O_2 that can be generated [38]. Furthermore, note

217 that at U = 11.9 cm s^{-1}, the maximum H_2O_2 concentration achieved (0.92 mM at 60 min) was
218 almost three-fold lower than that reached at the highest U = 79.6 cm s^{-1} (2.45 mM).

219 In the EF process, the addition of the Fe^{2+} catalyst has a negative effect on the H_2O_2
220 accumulation, as expected from its partial consumption by Fenton's reaction (3), which is
221 accelerated by the cyclic regeneration of Fe^{2+} through cathodic reduction of Fe^{3+} (reaction
222 (4)). This impact on H_2O_2 accumulation should be much more marked in the PEF process
223 because the photoreduction of the Fe^{3+} species through reactions (5) and (6) constitutes a
224 continuous source of Fe^{2+} that decomposes the H_2O_2. Fig. 3b shows the H_2O_2 accumulation
225 profiles obtained in EF and PEF at a catalyst concentration of 0.4 mM Fe^{2+}, at U = 79.6 cm
226 s^{-1}. As can be seen, the H_2O_2 accumulation in the EF process has a similar behavior to those
227 without Fe^{2+}, although reaching a lower H_2O_2 content at each sampling time because the
228 oxidant is partially destroyed via Fenton's reaction (3). The maximum concentration of 0.83
229 mM (28.3 mg L^{-1}) was attained at 60 min; a comparison with the trial at the same U of Fig.
230 3a reveals that 63% of the accumulated H_2O_2 is consumed upon reaction with Fe^{2+}. On the
231 other hand, in the PEF process, it can be observed that H_2O_2 was only detected from 15 min
232 of electrolysis, thereby following a gradual increase to reach a final concentration of 0.12
233 mM (3.93 mg L^{-1}), which represents only 5% of the final H_2O_2 concentration accumulated in
234 the trial without catalyst and UVA radiation. Such drastic decay in the H_2O_2 accumulation
235 supports the feasibility of photoreduction reactions (5) and (6) in an RCE set-up, which is
236 demonstrated for the first time, suggesting that PEF can be highly effective in destroying
237 organic pollutants because the H_2O_2 disappearance is known to be accompanied by the
238 production of $^{\bullet}OH$.

239 *3.2 Degradation of ampicillin by AO-H_2O_2, EF and PEF processes*

240 The ability of three different EAOPs with cathodic H_2O_2 production, namely AO-H_2O_2,
241 EF and PEF processes, to degrade ampicillin was first compared. As can be seen in Fig. 4a,
242 which highlights the AMP concentration decays over time, the complete drug elimination
243 was feasible in the three systems, although in the timescale of the electrolytic trials, it was
244 only achieved in the Fenton-based EAOPs. The fastest degradation occurred in the PEF
245 process, requiring 10 min, being slower in EF (20 min) and attaining an incomplete removal
246 (78% at 60 min) in AO-H_2O_2. The three decay trends could be adjusted to pseudo-first-order
247 kinetics, yielding apparent rate constants (k_1) with values of 3.6×10^{-2} (R^2 = 0.99), 2.1×10^{-1}
248 (R^2 = 0.98) and 4.2×10^{-1} min^{-1} (R^2 = 0.96) obtained in AO-H_2O_2, EF and PEF process,
249 respectively. The 2-fold faster destruction of AMP by PEF as compared to EF confirms the
250 occurrence and influential role of reactions (5) and (6) to enhance the degradation process.
251 This is further corroborated from Fig. 4b, which shows the time course of the normalized
252 Fe^{2+} concentration throughout the EF and PEF treatments; in PEF, the catalyst concentration
253 was maintained quite constant, close to its initial value thanks to its continuous and quick
254 photoregeneration from photodecarboxylation and photo-Fenton reactions (5) and (6),
255 respectively. On the other hand, a slight decrease in the Fe^{2+} content was obtained in EF,
256 although the cathodic regeneration from reaction (4) ensured that about 60-65% of the initial
257 Fe^{2+} content was always available to promote Fenton's reaction. Considering the Fe_{total}
258 profiles depicted in Fig. 4c, the missing 35-40% of Fe^{2+} along the EF trial may be partly
259 (~20-25% throughout the EF assay) explained by both the loss of soluble iron and the
260 generation of stable Fe(III)-carboxylate complexes not detectable spectrophotometrically.
261 Therefore, this means that the rest of the soluble iron (~15%) was in the form of
262 hydroxocomplexes of Fe^{3+} ion, which accumulated before being cathodically reduced. Such

accumulation of Fe^{3+} as part of diverse complexes accounts for the lower oxidation power of the EF process. In Fig. 4c, note that the absence of iron precipitates or stable Fe(III)-carboxylate complexes in PEF treatment is confirmed by the high stability of Fe_{total} (> 97%). In conclusion, the greater catalyst regeneration in PEF justifies the observed oxidation power in the order: PEF > EF > AO-H_2O_2.

3.3 Influence of the main experimental parameters on the antibiotic degradation

At his point, it is convenient to remind, as stated above, that the cathodically-generated H_2O_2 determines the extent and effectiveness of Fenton's reaction (3), directly influencing the AMP degradation. Since a new electrochemical reactor for H_2O_2 Electrosynthesis in the context of Fenton-based EAOPs is tested for the first time, it is essential to undertake a systematic study to optimize the most critical parameters to apply the PEF process whose superiority has been demonstrated above.

First, the effect of the initial Fe^{2+} concentration was evaluated. In more conventional stirred tanks and filter-press cells equipped with C-PTFE carbon cloth as the cathode, the optimum Fe^{2+} content has been established within the range 0.5-1.0 mM [20,21]. Based on this and taking into account the excellent regeneration ability of the PEF process, the effect of Fe^{2+} concentration was investigated in a lower range (0.3-0.6 mM). In Fig. 5a, the influence of the catalyst concentration on the drug removal is depicted. As can be noticed, a quicker elimination is attained when the concentration is increased from 0.3 mM to 0.4 mM, whereupon a further increase becomes detrimental. More specifically, the antibiotic disappears at 15, 10, 13 and 20 min employing initial Fe^{2+} concentrations of 0.3, 0.4, 0.5 and 0.6 mM, respectively. The slower elimination at $[Fe^{2+}]_0 > 0.4$ mM is attributed to the parasitic reaction (12) occurring between the catalyst and $^{\bullet}OH$. Worth reminding from Fig. 3b, no

H_2O_2 accumulation was observed at electrolysis time shorter than 15 min at U = 79.6 8 cm s^{-1} in the PEF process when an initial concentration of 0.4 mM Fe^{2+} was employed, which suggests that at Fe^{2+} concentration of 0.5 mM or greater the catalyst is found in excess, largely promoting reaction (12). The apparent rate constant (k_1) had values of 2.3×10^{-1} (R^2 = 0.98), 4.2×10^{-1} (R^2 = 0.96), 3.6×10^{-1} (R^2 = 0.97) and 1.8×10^{-1} min^{-1} (R^2 = 0.97) at Fe^{2+} concentrations rising from 0.3 to 0.6 mM. Moreover, the behavior of the Fe^{2+} concentration along the PEF treatment (Fig. 5b) evidences that at 0.4 mM Fe^{2+} the total catalyst regeneration is always ensured by photolytic and electrochemical reactions, whereas at higher initial contents some of the iron is not in the form of Fe^{2+}. This is especially evident at 0.6 mM Fe^{2+}, since only 50% of the species were present from 40 min, thus confirming the negative effect of the reaction (12). In agreement with the profiles of Fig. 5b, the Fe_{total} concentration shown in Fig. 5c is very stable and close to the initial one in the assay with 0.4 mM Fe^{2+}, whereas the catalyst content becomes more unstable and tends to decrease when rising the initial Fe^{2+} concentration. At 0.6 mM Fe^{2+}, around 20-30% of Fe_{total} could not be identified, plausibly due to the accumulation of a large amount of very refractory Fe(III)-carboxylate complexes that are slowly reduced.

$$Fe^{2+} + {}^{\bullet}OH \rightarrow Fe^{3+} + OH^{-} \qquad (12)$$

The second relevant parameter to be optimized was the peripheral velocity. As demonstrated in Fig. 3a, hydrodynamics has a crucial role in RCE reactors because mass transport is largely promoted as the rotation (i.e., peripheral velocity) is increased. Fig. 6a shows that the rise in U contributes to accelerate the AMP elimination in the PEF process, being the removal complete in all the tested U range; it was achieved after 30 min at U = 11.9 cm s^{-1}, only requiring 10 min at the greatest U = 79.6 cm s^{-1}. Alongside the higher

309 concentration of H_2O_2 accumulated at U = 79.6 cm s^{-1} (Fig. 3a) as a result of the improved
310 mass transport towards the coated RCE, the greater turbulence in the bulk solution favors the
311 interaction between $^{\bullet}OH$ produced from Fenton's reaction and AMP. In these trials,
312 gradually greater k_1-values of 1.1×10^{-1} (R^2 = 0.98), 1.3×10^{-1} (R^2 = 0.98), 1.4×10^{-1} (R^2 = 0.98),
313 2.5×10^{-1} (R^2 = 0.98) and 4.2×10^{-1} min^{-1} (R^2 = 0.96) at rising U values between 11.9 and 79.6
314 cm s^{-1} were determined. Furthermore, the improvement of mass transport toward the central
315 cathode can be corroborated by the Fe^{2+} concentration profiles depicted in Fig. 6b. Despite
316 the fact that UVA photons promote the fast photoreduction of free and complexed Fe(III) via
317 reactions (5) and (6), the simultaneous cathodic reduction of all these Fe(III) species is known
318 to have a very positive impact as well [42]. This means that the increase of U enhances the
319 mass transport of hydrated Fe^{3+} and the Fe(III) complexes, favoring the Fe^{2+} regeneration.
320 The Fe^{2+} concentration fluctuated substantially during the electrolysis and decayed by 15-
321 20% at U ≤ 39.8 cm s^{-1}, whereas it was kept quite constant and close to the initial value at
322 greater U. In particular, at the highest velocity U = 79.6 cm s^{-1}, the Fe^{2+} concentration was
323 always over 95%. It is also remarkable that the total iron concentration was higher than 90%
324 regardless of the peripheral velocity imposed to the coated RCE, confirming that the
325 enhanced mass transport of Fe^{3+} and the Fe(III)-organic complexes toward the cathode
326 surface favors the Fe^{2+} electro-regeneration (Fig. 6c). Therefore, the progressively greater
327 contribution of reaction (4) at higher U allows explaining the accelerated drug degradation
328 discussed from Fig. 6a.

329 Finally, the effect of the initial antibiotic concentration was evaluated within the range
330 5-15 mg L^{-1} to assess the overall power of the PEF process a U = 79.6 cm s^{-1}. From the results
331 shown in Fig. 7a, it can be observed that the fastest drug elimination was achieved at 5 mg

L^{-1} AMP, only needing 7 min for complete removal, whereas this was feasible after 10 and 20 min at higher drug contents of 10 and 15 mg L^{-1}, respectively. The k_1 determined for these three trials were 3.6-4.2×10^{-1} (R^2 = 0.99) at 5-10 mg L^{-1} AMP, and 1.7×10^{-1} (R^2 = 0.95) at 15 mg L^{-1}. Furthermore, Fig. 7b shows the catalyst behavior during these trials, which highlights that the optimum Fe^{2+} regeneration occurs at 10 mg L^{-1} AMP. Such a good Fe^{2+} recycling accounts for the much faster AMP degradation as compared to the trial using 15 mg L^{-1} AMP (Fig. 7a). Conversely, at the lowest drug content (5 mg L^{-1} AMP), the much smaller number of drug molecules could not be degraded at a significantly quicker rate (Fig. 7a) because of the decreasing Fe^{2+} concentration once the drug disappeared (Fig. 7b). This can be explained by the preferential consumption of $^{\bullet}OH$ through reaction with Fe^{2+} because of the lack of sufficient organic molecules. This reaction (12) yields mainly Fe^{3+}, as can be deduced from the very stable Fe_{total} concentration evidenced in Fig. 7c. A more oscillating profile, always corresponding to a lower amount of accumulated Fe^{2+} (decay of at least 40%), is observed at 15 mg L^{-1} AMP (Fig. 7b). However, total iron was kept quite constant throughout the trial.

A summary of the data obtained from PEF degradation trials can be found in Table 1. Note that the mineralization of the organic matter contained in the solutions followed a similar trend as compared to those of the AMP removals. The percentages of TOC abatement increased from 56% to 68% when rising from 11.9 to 79.6 cm s^{-1}. The photodecarboxylation reaction (5) contributes remarkably to the very large mineralization achieved in a short time of 60 min. It is also noticeable that the fastest decontamination, reaching 72% in only 30 min, was obtained in the trial performed with 5 mg L^{-1} AMP and 0.4 mM Fe^{2+} at 79.6 cm s^{-1}, with an energy consumption of 0.201 kWh (g TOC)$^{-1}$. The MCE ranged from 2.8% to 6.4%, owing to the low AMP concentrations under study. These low MCE values confirm the negative effect of reaction (12). The EC_{TOC} values were kept between 0.14 and 0.26 kWh (g TOC)$^{-1}$.

Here, it must be mentioned that, although the RCE reactor does not require a compressor to produce the H_2O_2, it requires energy to drive the electric motor that rotates the RCE, representing a quarter of the electrolytic energy consumption needed in the PEF process. In EF-related processes, the cost of electricity required tu operate the compressor is rarely reported. In a recent review on PEF process by Brillas [1], the EC_{TOC} for treatments made with filter-press cells attained values of 0.19-0.68 kWh (g TOC)$^{-1}$, which are similar to those obtained in the present study. Unfortunately, the energy consumed by the air compressor was not reported, but its inclusion in the calcualtions would substantially increase the energy costs.

Worth mentioning, the size of the O_2 bubbles as well as the thickness of the diffusion layer (δ) may play a crucial role in the H_2O_2 electrosynthesis [43] and, consequently, in the PEF performance. In the RCE reactor, the control of the electrolytic O_2 bubble size (preferably micro or nano) and δ mainly depends on the current density and the angular velocity of the RCE. Nonetheless, these aspects would require a deeper and focused experimental and computational fluid dynamic analysis.

3.4 Time course of carboxylic acids and inorganic ions

The carboxylic acids and inorganic ions generated during the antibiotic treatment were identified and quantified employing the experimental conditions described in Fig. 7, at 5 mg L^{-1} AMP. This antibiotic concentration was chosen in order to be as close as possible to a realistic value, leading to an accumulation of by-products that might be reasonable when treating an actual wastewater sample. Two short-chain linear aliphatic acids, oxalic and oxamic, were detected, and their accumulation profiles are shown in Fig. 8a. A continuous accumulation of both acids is observed from the beginning of the electrolysis, with oxalic

379 acid rising up to 1.5 mg L^{-1} at 30 min. This trend informs about the considerable refractoriness
380 of this aliphatic acid in a medium in which homogeneous $^{\bullet}OH$ is produced from reaction (3)
381 [33]. A similar behavior is presented by oxamic acid, as it accumulates throughout the
382 entirety of the electrolysis until a value of 1.35 mg L^{-1} is finally attained. It is worth noticing
383 that a quasi-plateau of oxamic acid concentration is achieved after 15 min of electrolysis. At
384 that time, 77% of the total N contained in AMP has already been converted into this acid,
385 alongside ammonium and nitrate ions, discussed below, which limits a greater accumulation
386 of oxamic acid. The final equivalent TOC concentrations from both acids are 0.40 mg L^{-1}
387 from oxalic and 0.36 mg L^{-1} TOC from oxamic, which represent 99% of the residual solution
388 TOC at the end of the treatment. Note that the complete disappearance of both acids was not
389 feasible under the tested conditions, in contrast to their reported quick photodegradation by
390 PEF [1,25,41], because of their presence as non-photoactive Fe(II)-carboxylate complexes.
391 On the other hand, Fig. 8b shows the evolution of inorganic ions generated during the
392 electrolysis. As can be seen, nitrate was continuously accumulated, owing to the high
393 oxidation power of the PEF process that allows converting the N-species into nitrate. In
394 contrast, ammonium almost reached a plateau from 15 min, which means that most N-species
395 were oxidized to nitrate. The C-PTFE carbon cloth cathode is so efficient to reduce O_2 to
396 H_2O_2 that it is almost unable to reduce other species such as nitrate [20]. The final
397 concentrations of nitrate and ammonium at 30 min were 0.94 mg L^{-1} (0.21 mg L^{-1} N), and
398 0.22 mg L^{-1} (0.17 mg L^{-1} N), respectively, which added to the final equivalent N content from
399 oxamic acid (0.21 mg L^{-1} N) approximately account for a 99% of the total N contained in the
400 antibiotic.

4. Conclusions

Aqueous solutions of the antibiotic ampicillin were successfully treated in a batch reactor equipped with a C-PTFE carbon cloth-coated RCE that produces H_2O_2 from anodically-produced O_2. The feasibility of H_2O_2 electrosynthesis without the need of a compressor, in sufficient amounts to sustain several EAOPs for water treatment, is demonstrated for the first time. Up to 83.3 mg L^{-1} H_2O_2 (~2.5 mM H_2O_2) were accumulated at 60 min at fixed E_{cath} = –0.45 V vs. SHE and U = 79.6 cm s^{-1}. The fastest degradation of solutions with 10 mg L^{-1} AMP was established under PEF conditions, operating at 0.4 mM Fe^{2+}, U = 79.6 cm s^{-1} and E_{cath} = –0.45 V to completely remove AMP in 10 min. In addition, a TOC abatement of 68% was achieved at 60 min, with EC_{TOC} of 0.211 kW h (g TOC)$^{-1}$. The residual TOC mainly corresponded to oxalic and oxamic acids. An important finding that supports the convenience of using an RCE to run the PEF process is that this reactor configuration decreases the electrolysis time owing to the outstanding mass transport. For example, filter-press type reactors typically require from 4 to 8 h to mineralize pharmaceuticals at a similar concentration to that assessed here. In addition, the results obtained in this work suggest that a sustainable treatment of antibiotics in water is feasible by using an RCE reactor with solar radiation, thus eliminating the cost of both the compressor and the lamp.

Acknowledgements

Funding from projects CIIC 203/2022 (University of Guanajuato, Mexico) and PID2019-109291RB-I00 (MCIN/AEI/10.13039/501100011033, Spain) is kindly acknowledged.

References

[1] E. Brillas, Progress of homogeneous and heterogeneous electro-Fenton treatments of antibiotics in synthetic and real wastewaters. A critical review on the period 2017–2021, Sci. Total Environ. 819 (2022) 153102. DOI: 10.1016/j.scitotenv.2022.153102

[2] J. Davies, D. Davies, Origins and evolution of antibiotic resistance, Microl. Mol. Biol. Rev. 74 (2010) 417-433. DOI: 10.1128/MMBR.00016-10

[3] S. Bombaywala, A. Mandpe, S. Paliya, S. Kumar, Antibiotic resistance in the environment: a critical insight on its occurrence, fate, and eco-toxicity, Environ. Sci. Pollut. Res. 28 (2021) 24889-24916. DOI: 10.1007/s11356-021-13143-x

[4] S. Fekadu, E. Alemayehu, R. Dewil, B. Van der Bruggen, Pharmaceuticals in freshwater aquatic environments: A comparison of the African and European challenge, Sci. Total Environ. 654 (2019) 324-337. DOI: 10.1016/j.scitotenv.2018.11.072

[5] U. Szymańska, M. Wiergowski, I. Sołtyszewski, J. Kuzemko, G. Wiergowska, M.K. Woźniak, Presence of antibiotics in the aquatic environment in Europe and their analytical monitoring: Recent trends and perspectives, Microchem. J. 147 (2019) 729-740. DOI: 10.1016/j.microc.2019.04.003

[6] P. Kairigo, E. Ngumba, L.R. Sundberg, A. Gachanja, T. Tuhkanen, Occurrence of antibiotics and risk of antibiotic resistance evolution in selected Kenyan wastewaters, surface waters and sediments, Sci. Total Environ. 720 (2020) 137580. DOI: 10.1016/j.scitotenv.2020.137580

[7] H.Q. Anh, T.P.Q. Le, N.D. Le, X.X. Lu, T.T. Duong, J. Garnier, E. Rochelle-Newall, S. Zhang, N.H. Oh, C. Oeurng, C. Ekkawatpanit, T.D. Nguyen, Q.T. Nguyen, T.D.

Nguyen, T.N. Nguyen, T.L. Tran, T. Kunisue, R. Tanoue, S. Takahashi, T.B. Minh, H.T. Le, T.N.M. Pham, T.A.H. Nguyen, Antibiotics in surface water of East and Southeast Asian countries: A focused review on contamination status, pollution sources, potential risks, and future perspectives, Sci. Total Environ. 764 (2021) 142865. DOI: 10.1016/j.scitotenv.2020.142865

[8] C. Afonso-Olivares, Z. Sosa-Ferrera, J.J. Santana-Rodríguez, Occurrence and environmental impact of pharmaceutical residues from conventional and natural wastewater treatment plants in Gran Canaria (Spain), Sci. Total Environ. 599-600 (2017) 934-943. DOI: 10.1016/j.scitotenv.2017.05.058

[9] A. Bielen, A. Šimatović, J. Kosić-Vukšić,I. Senta, M. Ahel, S. Babić, T. Jurina, J.J. González Plaza, M. Milaković, N. Udiković-Kolić, Negative environmental impacts of antibiotic-contaminated effluents from pharmaceutical industries, Water Res. 126 (2017) 79-87. DOI: 10.1016/j.watres.2017.09.019

[10] J. Wang, L. Chu, L. Wojnárovits, E. Takács, Occurrence and fate of antibiotics, antibiotic resistant genes (ARGs) and antibiotic resistant bacteria (ARB) in municipal wastewater treatment plant: An overview, Sci. Total Environ. 744 (2020) 140997. DOI: 10.1016/j.scitotenv.2020.140997

[11] Z. Lin, T. Yuan, L. Zhou, S. Cheng, X. Qu, P. Lu, Q. Feng, Impact factors of the accumulation, migration and spread of antibiotic resistance in the environment, Environ. Geochem. Health 43 (2021) 1741-1758. DOI: 10.1007/s10653-020-00759-0

[12] D.G.J. Larsson, C.F. Flach, Antibiotic resistance in the environment, Nat. Rev. Microbiol. 20 (2022) 257-269. DOI: 10.1038/s41579-021-00649-x

[13] M. Savin, G. Bierbaum, J.A. Hammerl, C. Heinemann, M. Parcina, E. Sib, A. Voigt, J. Kreyenschmidt, Antibiotic-resistant bacteria and antimicrobial residues in wastewater and process water from German pig slaughterhouses and their receiving municipal wastewater treatment plants, Sci. Total Environ. 727 (2020) 138788. DOI: 10.1016/j.scitotenv.2020.138788

[14] K. Wang, T. Zhuang, Z. Su, M. Chi, H. Wang, Antibiotic residues in wastewaters from sewage treatment plants and pharmaceutical industries: Occurrence, removal and environmental impacts, Sci. Total Environ. 788 (2021) 147811. DOI: 10.1016/j.scitotenv.2021.147811

[15] L. Feng, E.D. van Hullesbusch, M.A. Rodrigo, G. Esposito, M.A. Oturan, Removal of residual anti-inflammatory and analgesic pharmaceuticals from aqueous systems by electrochemical advanced oxidation processes. A review, Chem. Eng. J. 228 (2013) 944-964. DOI: 10.1016/j.cej.2013.05.061

[16] E. Brillas, I. Sirés, Electrochemical removal of pharmaceuticals from water streams: Reactivity elucidation by mass spectrometry, TrAC-Trends Anal. Chem. 70 (2015) 112-121. DOI: 10.1016/j.trac.2015.01.013

[17] A.J. Dos Santos, M.S. Kronka, G.V. Fortunato, M.R.V. Lanza, Recent advances in electrochemical water technologies for the treatment of antibiotics: A short review, Curr. Opinion Electrochem. 26 (2021) 100674. DOI: 10.1016/j.coelec.2020.100674

[18] J. Wang, R. Zhuan, Degradation of antibiotics by advanced oxidation processes: An overview, Sci. Total Environ. 701 (2020) 135023. DOI: 10.1016/j.scitotenv.2019.135023

[19] R.Y. Krishnan, S. Manikandan, R. Subbaiya, M. Biruntha, M. Govarthanan, N. Karmegam, Removal of emerging micropollutants originating from pharmaceuticals

and personal care products (PPCPs) in water and wastewater by advanced oxidation processes: A review, Environ. Technol. Innov. 23 (2021) 101757. DOI: 10.1016/j.eti.2021.101757

[20] G. Daniel, Y. Zhang, S. Lanzalaco, F. Brombin, T. Kosmala, G. Granozzi, A. Wang, E. Brillas, I. Sirés, C. Durante, Chitosan-derived nitrogen-doped carbon electrocatalyst for a sustainable upgrade of oxygen reduction to hydrogen peroxide in UV-assisted electro-Fenton water treatment, ACS Sustain. Chem. Eng. 8 (2020) 14425-14440. DOI: 10.1021/acssuschemeng.0c04294

[21] Y. Zhang, G. Daniel, S. Lanzalaco, A.A. Isse, A. Facchin, A. Wang, E. Brillas, C. Durante, I. Sirés, H_2O_2 production at gas-diffusion cathodes made from agarose-derived carbons with different textural properties for acebutolol degradation in chloride media, J. Hazard. Mater. 423 (2022) 127005. DOI: 10.1016/j.jhazmat.2021.127005

[22] A. Galia, S. Lanzalaco, M.A. Sabatino, C. Dispenza, O. Scialdone, I. Sirés, Crosslinking of poly(vinylpyrrolidone) activated by electrogenerated hydroxyl radicals: A first step towards a simple and cheap synthetic route of nanogel vectors, Electrochem. Commun. 62 (2016) 64-68. DOI: 10.1016/j.elecom.2015.12.005

[23] O. Ganzenko, C. Trellu, N.Oturan, D. Huguenot, Y. Péchaud, E.D. van Hullebusch, M.A. Oturan, Electro-Fenton treatment of a complex pharmaceutical mixture: Mineralization efficiency and biodegradability enhancement, Chemosphere 253 (2020) 126659. DOI: 10.1016/j.chemosphere.2020.126659

[24] A.A. Márquez, I. Sirés, E. Brillas, J.L. Nava, Mineralization of Methyl Orange azo dye by processes based on H_2O_2 electrogeneration at a 3D-like air-diffusion cathode, Chemosphere 259 (2020) 127466. DOI: 10.1016/j.chemosphere.2020.127466

[25] M.F. Murrieta, E. Brillas, J.L. Nava, I. Sirés, Photo-assisted electrochemical production of HClO and Fe^{2+} as Fenton-like reagents in chloride media for sulfamethoxazole degradation, Sep. Purif. Technol. 250 (20209 117236. DOI: 10.1016/j.seppur.2020.117236

[26] D. Clematis, M. Panizza, Electro-Fenton, solar photoelectro-Fenton and UVA photoelectro-Fenton: Degradation of Erythrosine B dye solution, Chemosphere 270 (2021) 129480. DOI: 10.1016/j.chemosphere.2020.129480

[27] C.D. Gamarra-Güere, D. Dionisio, G.O.S. Santos, M.R.V. Lanza, A.J. Motheo, Application of Fenton, Photo-Fenton and Electro-Fenton processes for the methylparaben degradation: a comparative study, J. Environ. Chem. Eng. 10 (2021) 106992. DOI: 10.1016/j.jece.2021.106992

[28] G. Coria, T. Pérez, I. Sirés, J.L. Nava, Mass transport studies during dissolved oxygen reduction to hydrogen peroxide in a filter-press electrolyzer using graphite felt, reticulated vitreous carbon and boron-doped diamond as cathodes, J. Electroanal. Chem. 757 (2015) 225-229. DOI: 10.1016/j.jelechem.2015.09.031

[29] T. Pérez, G. Coria, I. Sirés, J.L. Nava, A.R. Uribe, Electrosynthesis of hydrogen peroxide in a filter-press flow cell using graphite felt as air-diffusion cathode, J. Electroanal. Chem. 812 (2018) 54-58. DOI: 10.1016/j.jelechem.2018.01.054

[30] A. Xu, B. He, H. Yu, W. Han, J. Li, J. Shen, X. Sun, L. Wang, A facile solution to mature cathode modified by hydrophobic dimethyl silicon oil (DMS) layer for electro-Fenton processes: Water proof and enhanced oxygen transport, Electrochim. Acta 308 (2019) 158-166. DOI: 10.1016/j.electacta.2019.04.047

[31] J. Lu, X. Liu, Q. Chen, J. Zhou, Coupling effect of nitrogen-doped carbon black and carbon nanotube in assembly gas diffusion electrode for H_2O_2 electro-generation and

recalcitrant pollutant degradation, Sep. Purif. Technol. 265 (2021) 118493. DOI: 10.1016/j.seppur.2021.118493

[32] J. Wang, C. Li, M. Rauf, H. Luo, X. Sun, Y. Jiang, Gas diffusion electrodes for H_2O_2 production and their applications for electrochemical degradation of organic pollutants in water: A review, Sci. Total Environ. 759 (2021) 143459. DOI: 10.1016/j.scitotenv.2020.143459

[33] G. Coria, I. Sirés, E. Brillas, J.L. Nava, Influence of the anode material on the degradation of naproxen by Fenton-based electrochemical processes, Chem. Eng. J. 304 (2016) 817-825. DOI: 10.1016/j.cej.2016.07.012

[34] N. Klidi, D. Clematis, M.P. Carpanese, A. Gadri, S. Ammar, M. Panizza, Electrochemical oxidation of crystal violet using a BDD anode with a solid polymer electrolyte, Sep. Purif. Technol. 208 (2019) 178-183. DOI: 10.1016/j.seppur.2018.03.042

[35] W. Zhou, L. Rajic,Y. Zhao, J. Gao, Y. Qin, A.N. Alshawabkeh, Rates of H_2O_2 electrogeneration by reduction of anodic O_2 at RVC foam cathodes in batch and flow-through cells, Electrochim. Acta 277 (2018) 185-196. DOI: 10.1016/j.electacta.2018.04.174

[36] O.M. Cornejo, I. Sirés, J.L. Nava, Electrosynthesis of hydrogen peroxide sustained by anodic oxygen evolution in a flow-through reactor, J. Electroanal. Chem. 873 (2020) 114419. DOI: 10.1016/j.jelechem.2020.114419

[37] X. Wang, P. Cao, K. Zhao, S. Chen, H. Yu, X. Quan, Flow-through heterogeneous electro-Fenton system based on the absorbent cotton derived bulk electrode for refractory organic pollutants treatment, Sep. Purif. Technol. 276 (2021) 119266. DOI: 10.1016/j.seppur.2021.119266

563 [38] O.M. Cornejo, I. Sirés, J.L. Nava, Cathodic generation of hydrogen peroxide
564 sustained by electrolytic O_2 in a rotating cylinder electrode (RCE) reactor.
565 Electrochim. Acta 404 (2021) 139621. DOI: 10.1016/j.electacta.2021.139621
566 [39] Z.G. Aguilar, O. Coreño, M. Salazar, I. Sirés, E. Brillas, J.L. Nava, Ti|Ir–Sn–Sb oxide
567 anode: Service life and role of the acid sites content during water oxidation to
568 hydroxyl radicals, J. Electroanal. Chem. 820 (2018) 82-88. DOI:
569 10.1016/j.jelechem.2018.04.053
570 [40] AWWA, AWWA, WEF, Standard Methods for the Examination of Water and
571 Wastewater, 21st ed., American Public Health Association, Washington D.C, 2005.
572 [41] T. Pérez, I. Sirés, E. Brillas, J.L. Nava, Solar photoelectro-Fenton flow plant
573 modeling for the degradation of the antibiotic erythromycin in sulfate medium,
574 Electrochim. Acta 228 (2017) 45-56. DOI: 10.1016/j.electacta.2017.01.047
575 [42] I. Sirés, J.A. Garrido, R.M. Rodríguez, E. Brillas, N. Oturan, M.A. Oturan, Catalytic
576 behavior of the Fe^{3+}/Fe^{2+} system in the electro-Fenton degradation of the
577 antimicrobial chlorophene, Appl. Catal. B: Environ. 72 (2007) 382-394. DOI:
578 10.1016/j.apcatb.2006.11.016
579 [43] S. Qiu, W. Tang, S. Yang, J. Xie, D. Yu, O. Garcia-Rodriguez, J. Qu, S. Bai, F. Deng,
580 A microbubble-assisted rotary tubular titanium cathode for boosting Fenton's
581 reagents in the electro-Fenton process, J. Hazard. Mater. A 424 (2022) 127403. DOI:
582 10.1016/j.jhazmat.2021.127403

583 **Figure captions**

584 **Fig. 1.** Structural formula of AMP antibiotic (in its sodium salt form, as employed here).

585 **Fig. 2.** (a) Experimental set-up, including the UVA lamp that was turned on only in PEF
586 trials. (b) Top view of the RCE reactor.

587 **Fig. 3.** (a) Influence of peripheral velocity on the H_2O_2 concentration profile and (b)
588 accumulated H_2O_2 concentration during the EF and PEF treatments at 0.4 mM Fe^{2+} and U =
589 79.6 cm s^{-1}. Solution: 50 mM Na_2SO_4 at pH 3 and 298 ± 2 K. E_{cath} = –0.45 V vs. SHE.

590 **Fig. 4.** (a) Comparison of the normalized AMP concentration decays over the electrolysis
591 time upon application of AO-H_2O_2, EF and PEF treatments. Corresponding time course of
592 normalized (b) Fe^{2+} concentration and (c) total iron concentration in the EF and PEF
593 treatments of a solution of 10 mg L^{-1}AMP + 50 mM Na_2SO_4 at pH 3 and 298 ± 2 K.
594 Conditions: E_{cath} = –0.45 V vs. SHE, U = 79.6 cm s^{-1}. In EF and PEF, Fe^{2+} was initially added
595 at a concentration of 0.4 mM.

596 **Fig. 5.** Influence of initial Fe^{2+} concentration on normalized (a) AMP concentration decay,
597 (b) Fe^{2+} concentration and (c) total iron concentration over the electrolysis time during the
598 PEF treatment of 10 mg L^{-1}AMP + 50 mM Na_2SO_4 at pH 3 and 298 ± 2 K. Conditions: E_{cath}
599 = –0.45 V vs. SHE, U = 79.6 cm s^{-1}.

600 **Fig. 6.** Influence of imposed U on normalized (a) AMP concentration decay, (b) Fe^{2+}
601 concentration and (c) total iron concentration over the electrolysis time during the PEF
602 treatment of 10 mg L^{-1}AMP + 50 mM Na_2SO_4 + 0.4 mM Fe^{2+} at pH 3 and T = 298 ± 2 K.
603 Conditions: E_{cath} = –0.45 V vs. SHE, U = 79.6 cm s^{-1}.

Fig. 7. Influence of AMP initial concentration on normalized (a) AMP concentration decay, (b) Fe^{2+} concentration and (c) total iron concentration over the electrolysis time during the PEF treatment of different concentrations of AMP in solutions containing 50 mM Na_2SO_4 + 0.4 mM Fe^{2+} at pH 3 and T = 298 ± 2 K. Conditions: E_{cath} = –0.45 V vs. SHE, U = 79.6 cm s^{-1}.

Fig. 8. Evolution of the concentration of (a) carboxylic acids and (b) inorganic ions during the elimination of the antibiotic AMP by PEF process. Same experimental conditions as those described in Fig. 7 at 5 mg L^{-1} AMP.

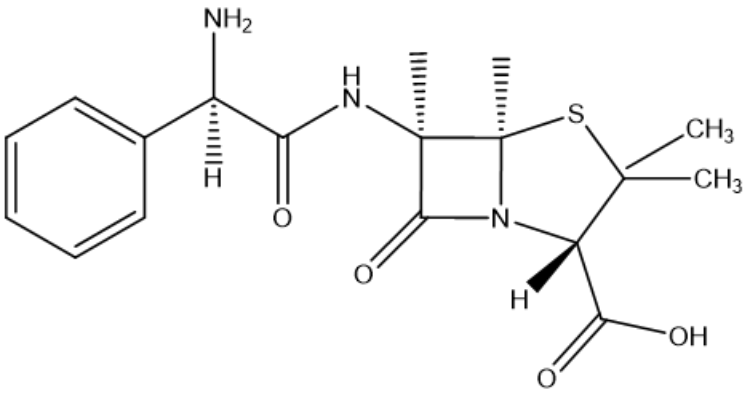

Fig. 1

619

620

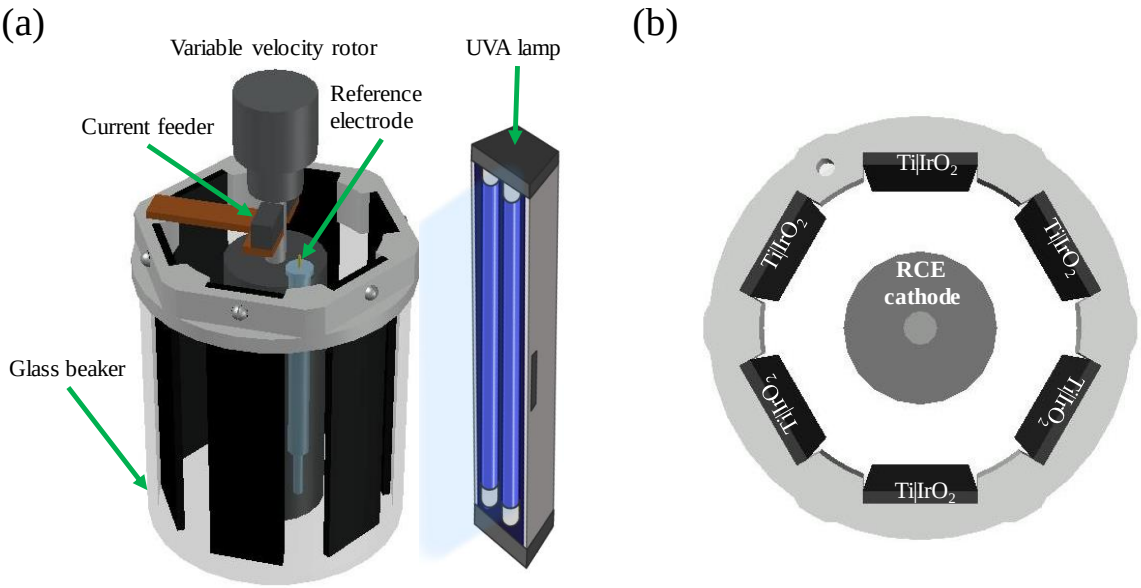

621

622

623

624

625 **Fig. 2**

626

627

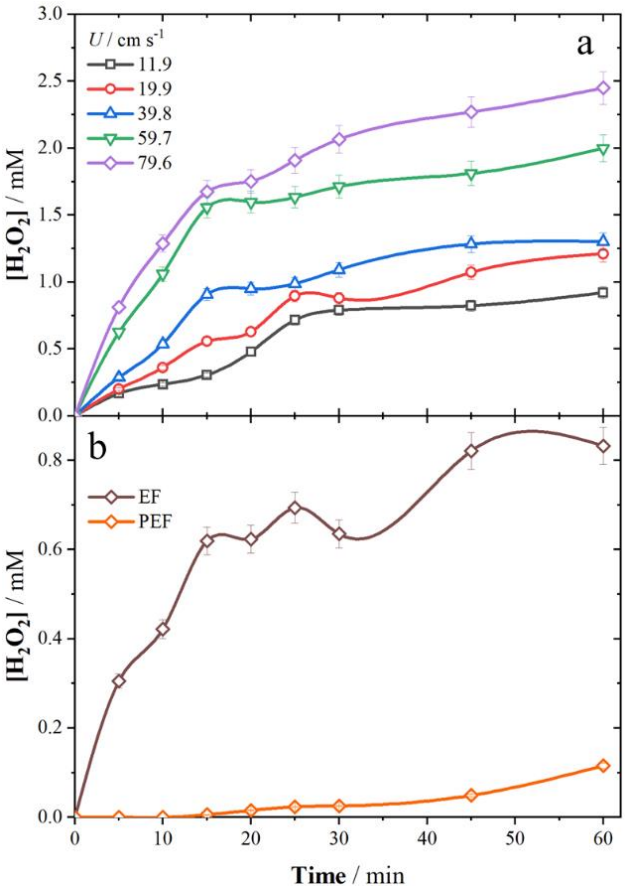

628

629

630

631

632 **Fig. 3**

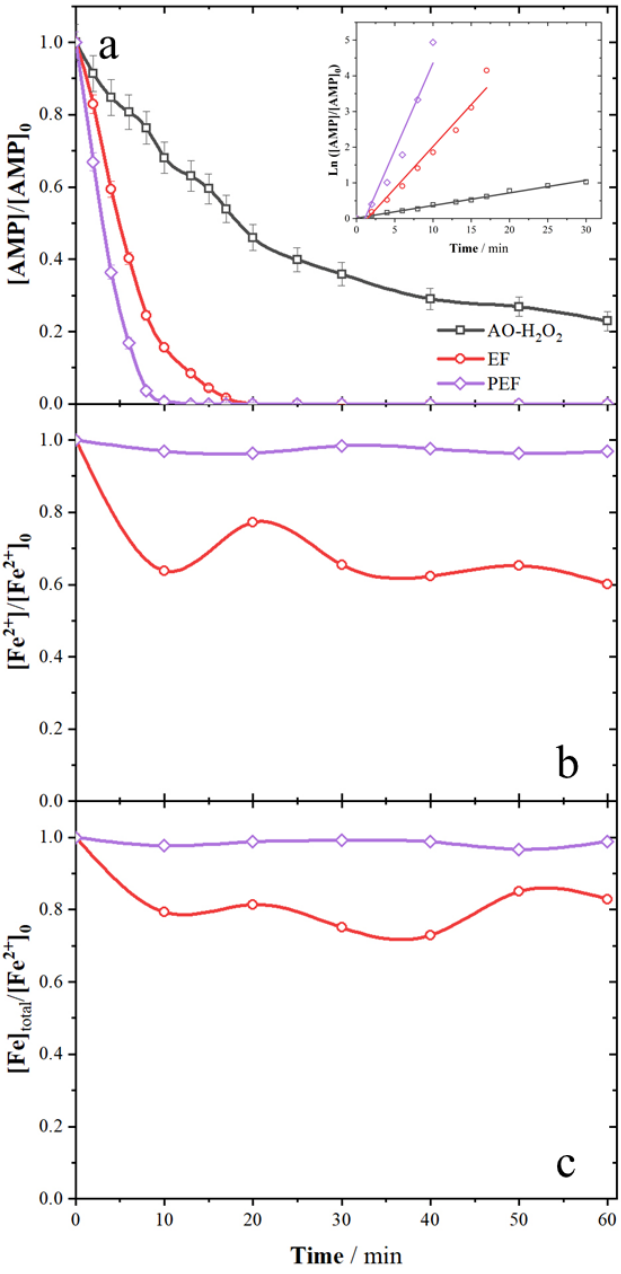
a
b
c
[AMP]/[AMP]0
[Fe2+]/[Fe2+]0
[Fe]total/[Fe2+]0
Ln ([AMP]/[AMP]0)
Time / min
AO-H2O2
EF
PEF
Time / min

Fig. 4

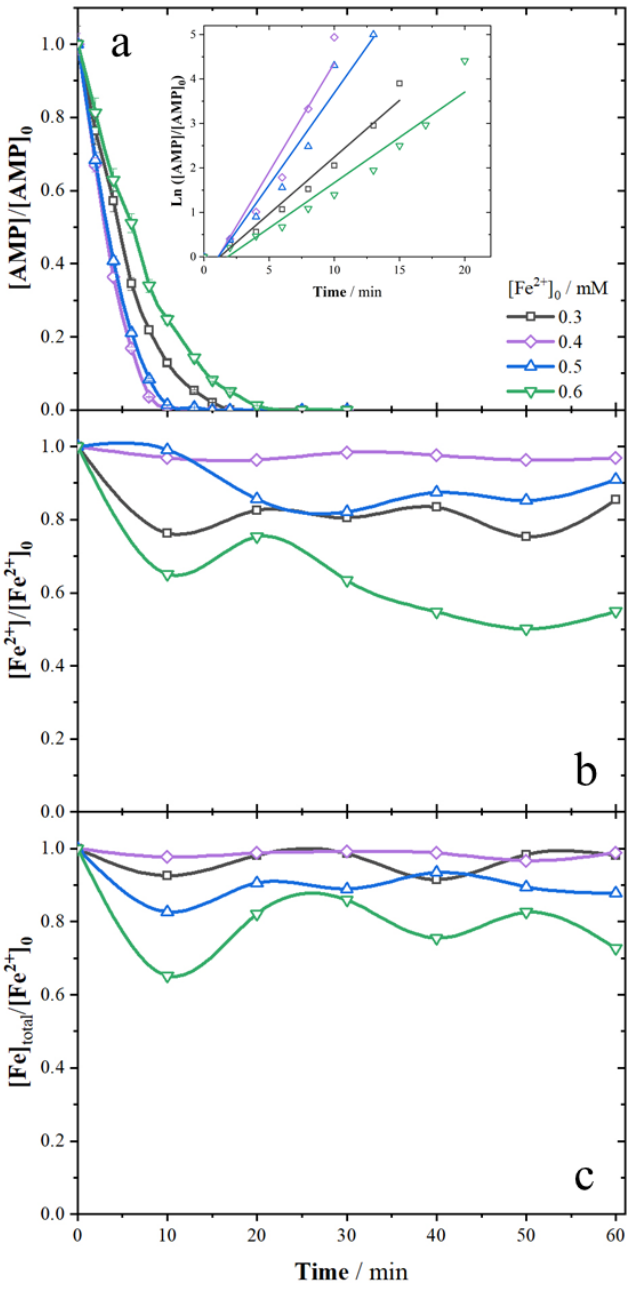
a
b
c
[AMP]/[AMP]0
[Fe2+]/[Fe2+]0
[Fe]total/[Fe2+]0
Ln ([AMP]/[AMP]0)
Time / min
[Fe2+]0 / mM
0.3
0.4
0.5
0.6

Fig. 5

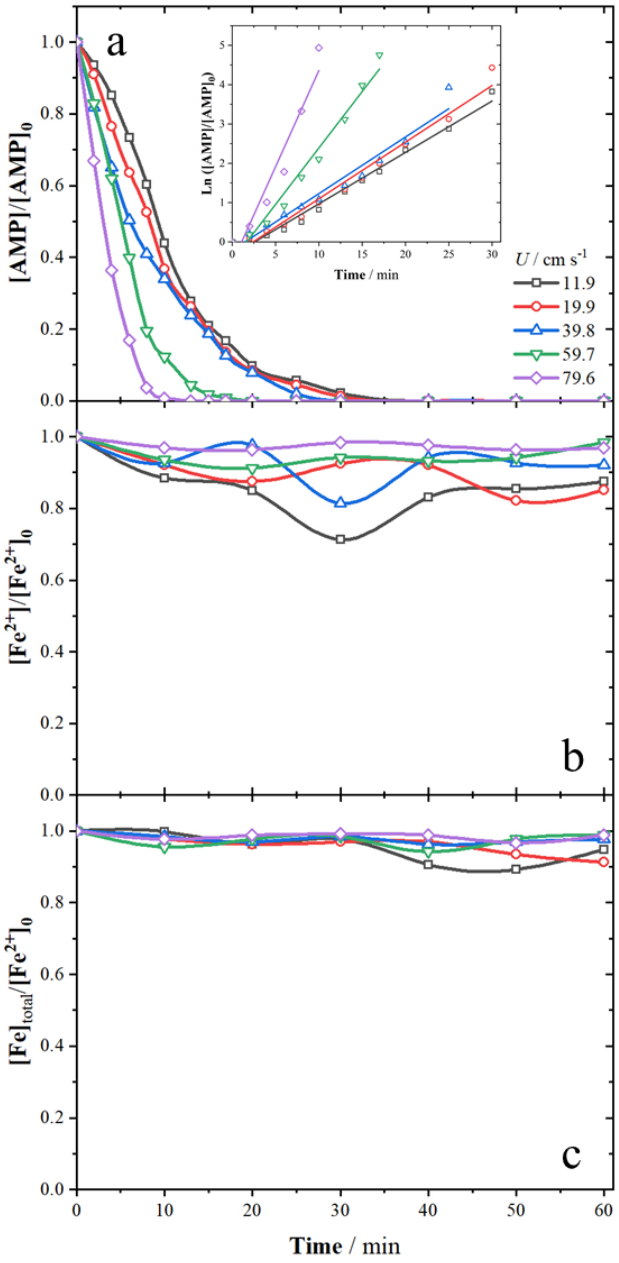
a
b
c
[AMP]/[AMP]0
[Fe2+]/[Fe2+]0
[Fe]total/[Fe2+]0
Ln ([AMP]/[AMP]0)
Time / min
U / cm s-1
11.9
19.9
39.8
59.7
79.6
Time / min

Fig. 6

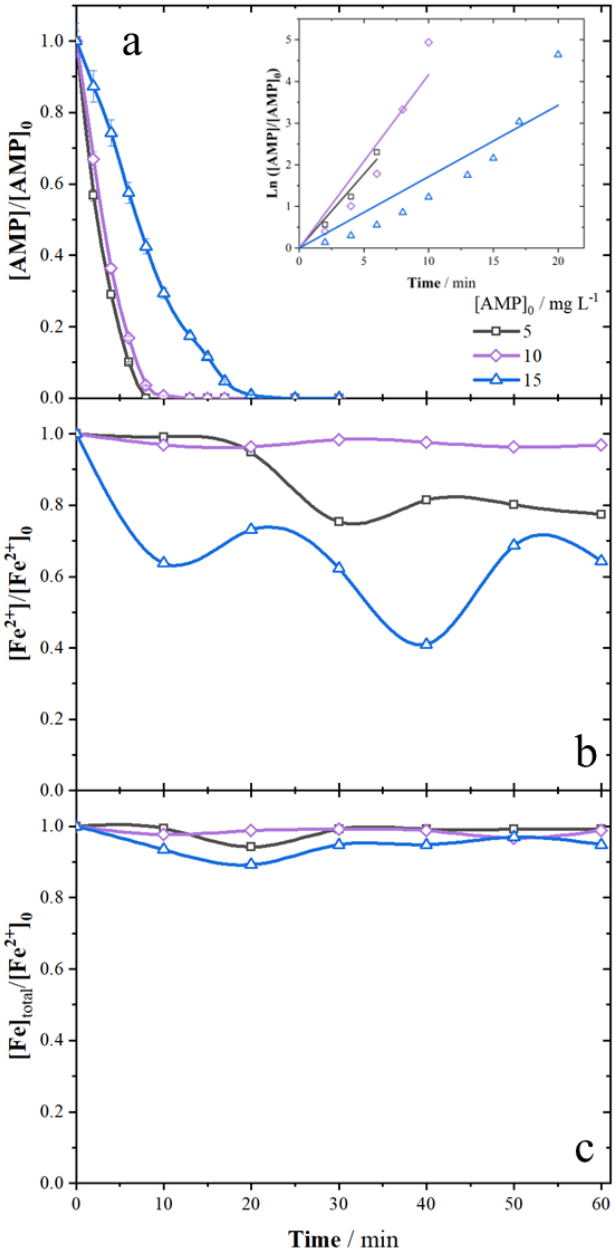
a
b
c
[AMP]/[AMP]0
[Fe2+]/[Fe2+]0
[Fe]total/[Fe2+]0
Ln ([AMP]/[AMP]0)
Time / min
[AMP]0 / mg L-1
5
10
15
Time / min

Fig. 7

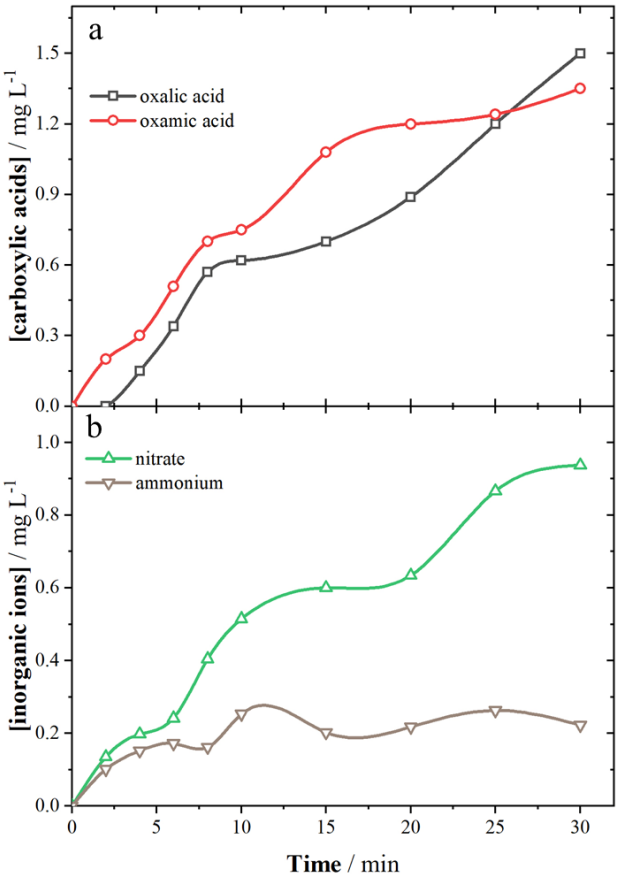
a
oxalic acid
oxamic acid
[carboxylic acids] / mg L-1
1.5
1.2
0.9
0.6
0.3
0.0
b
nitrate
ammonium
[inorganic ions] / mg L-1
1.0
0.8
0.6
0.4
0.2
0.0
0
5
10
15
20
25
30
Time / min

Fig. 8

668 **Table 1**

669 Summary of pseudo-first-order rate constants for AMP degradation by PEF process, and their
670 corresponding *R*-squared values, as well as the percentages of TOC removal and electrolytic
671 energy consumption per unit TOC mass for the trials performed in the RCE reactor.

U / cm s^{-1}	$[Fe^{2+}]_0$ / mM	$[AMP]_0$ / mg L^{-1}	k_1 / $\times 10^{-2}$ min^{-1}	R^2	% TOC removal	EC_{TOC} / kWh (g TOC)$^{-1}$	% MCE
11.9	0.4	10	1.1	0.98	56[a]	0.142	5.3
19.9	0.4	10	1.3	0.98	58[a]	0.165	4.7
39.8	0.4	10	1.4	0.98	57[a]	0.195	3.9
59.7	0.4	10	2.5	0.98	63[a]	0.203	3.3
79.6	0.3	10	2.3	0.98	63[a]	0.177	3.1
	0.4	5	3.6	0.99	72[b]	0.201	3.4
	0.4	10	4.2	0.96	68[a]	0.211	2.8
	0.4	15	1.7	0.93	37[a]	0.261	6.4
	0.5	10	3.6	0.97	66[a]	0.216	2.9
	0.6	10	1.8	0.97	60[a]	0.238	3.2

672 At [a]t = 60 min, and [b]t = 30 min.